Available online at www.sciencedirect.com

ScienceDirect

Procedia Structural Integrity 17 (2019) 105–114

Structural Integrity Procedia

www.elsevier.com/locate/procedia

ICSI 2019 The 3rd International Conference on Structural Integrity

Correlation between fractographic aspects and stress intensity factor in very high cycle fatigue

M.V. Pereira[a], M.C. Teixeira[a*], F. A. Darwish[b]

[a]*Department of Chemical and Materials Engineering, Catholic University of Rio de Janeiro, Rua Marques de São Vicente, 225, Rio de Janeiro, 22453-901, RJ, Brazil*

[b]*Department of Civil Engineering, Fluminense Federal University, Rua Passo da Patria,156, Niteroi, 24210-240, RJ, Brazil*

Abstract

Very high cycle fatigue (VHCF) tests carried out at high frequency made it possible for one to evaluate the behavior of materials, particularly steels, for fatigue lives exceeding 10^6 - 10^7 cycles in relatively short time intervals compared to conventional fatigue tests. This reduction in the test duration is due to the ultrasonic frequencies, usually situated in the range 15 - 30 kHz, provided by the test machines. In the VHCF regime, the fatigue crack tends to start internally or in subsurface from internal defects, intrinsic to the material. The evolution of fatigue cracks occurs in different stages: crack initiation, crack growth within the fish-eye, crack growth outside the fish-eye, and then final fracture. In addition, another phenomenon that may occur inside the fish-eye and nearby the initial defect, is known as fine granular area (FGA). VHCF tests of a crankshaft steel were performed at a frequency of 20 kHz and loading ratio of -1. The S-N curve indicates an increase in fatigue life as the applied stress decreases. The fracture surfaces analyzed have also indicated the presence of fish-eye which includes an FGA region. Aspects referring to fish-eye and FGA are presented and related to stress intensity factor (SIF).

Peer-review under responsibility of the ICSI 2019 organizers.

Keywords: VHCF; FGA; fish-eye; SIF;

* Corresponding author. Tel.: +55 21 3527-1237.
E-mail address: mclaract@gmail.com

2452-3216
Peer-review under responsibility of the ICSI 2019 organizers.
10.1016/j.prostr.2019.08.015

1. Introduction

The concepts of very high cycle fatigue (VHCF) associate the applied stresses with the number of cycles to failure in very long life ($N_f > 10^6$). This has become possible due to ultrasonic fatigue machines that work in high frequency (20 kHz). The ultrasonic fatigue tests reduced significantly the time and cost of fatigue testing, making it possible to understand the material behavior in very long life. In recent years, several researchers tested various materials and revealed that fatigue limit does not exist in many cases (Bathias (2007), Kazymyrovych (2008), Marines et al.(2003)). In addition, the origin of fatigue fracture of specimens in VHCF regime most often occurs internally or at subsurface defects and sometimes can start on the specimen surface similar to high and low cycle fatigue regimes. According to Bathias (2007) (Pyttel et al. (2011)), there are three main factors leading to crack nucleation in VHCF: (i) anisotropy, (ii) stress concentration, (iii) statistical conditions.

The fracture surface for internal crack initiation exhibits a circular region characterized by circular crack propagation, called fish-eye (Kazymyrovych (2009), Kazymyrovych (2008)). Furthermore, another region frequently appears in the fracture surface nearby the initial defect. Researchers generally lable this region with different denominations: fine granular area (FGA) by Sakai et.al.(2009)(Li et al. (2016)), optically dark area (ODA) by Murakami et.al. (2002)(Li et al. (2016)), granular bright area (GBF) by Shiozawa et.al.(2006)(Li et al. (2016))and rough surface area (RSA) by Ochi et.al (Ochi et al. (2002)). The denomination FGA used by Sakai el al. (2009) was adopted for the present work.

The mechanisms that act in the VHCF regime have been extensively studied by several researchers and various empirical equations were developed with the purpose of quantifying the size of the FGA and understanding which mechanical properties influence its formation.

The main aims of this work was to identify the fracture surface morphologies and to determine the FGA size by scanning electron microscopy (SEM) as well as digital image processing (DIP) and then compare the measured sizes with estimates made by empirical equations encountered in the literature. Finally, FGA and fish-eye sizes were used to calculate the stress intensity factor (SIF) at the boundary of these, two regions, in an effort to comprehend the transition from short to long cracks.

Nomenclature

φ_{FGA}	diameter of FGA by Yang. et al.
$\sqrt{A_{FGA}}$	FGA size parameter due to Liu et al.
$\sqrt{area_{FGA}}$	FGA size parameter due to Murakami et al.
d_{FGA}	diameter of FGA
σ_y	yield stress
σ_a	applied stress amplitude
σ_u	ultimate stress
E	modulus of elasticity
HV	Vickers hardness
ΔK_{FGA}	stress intensity factor range of FGA
$\Delta K_{fish\text{-}eye}$	stress intensity factor range of fish-eye
ΔK_{th}	fatigue crack propagation threshold
ΔK_{thR}	mechanical threshold for long cracks

2. Fracture surface interpretations

2.1. Fish-eye and roughness surface

Most fracture surfaces in VHCF regime present internal or subsurface crack initiation at nonmetallic inclusions. This type of initiation results in the formation of what is denominated fish-eye, which has a circular appearance and is responsible for circular crack propagation. Thus, crack propagation is divided into four stages (Fig.1): (i) crack initiation, (ii) crack growth within the fish-eye, (iii) crack growth outside the fish-eye and (iv) final fracture. In this way, the fish-eye boundary determines the final size of the circular fatigue crack propagation and the start of a different propagation mode (Kazymyrovych (2009), Kazymyrovych et al. (2010)). The final size is normally defined when the fish-eye edge reaches the surface.

The fracture surface of VHCF specimens usually exhibits a region nearby the initial defect characterized by rough morphology and generally denominated FGA. This region is described by several models, but its formation mechanism is not clear. Some researchers believe that the formation of such region is a part of the nucleation process and others interpret it as corresponding to crack growth (Li et al. (2015)). However, it is believed that FGA detains about 90% of the fatigue life, that is, the FGA defines the VHCF behavior, meaning that fatigue life increases as FGA size increases.

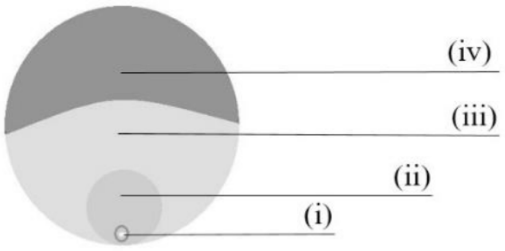

Fig. 1. Different stages for VHCF crack formation (adapted from V. Kazymyrovych illustration)(Kazymyrovych (2008); Kazymyrovych et al. (2010)).

According to Sakai et.al (2009) (Li et al. (2016)), the formation of FGA is divided in three stages. The first stage is related to a polygonization mechanism, where a fine granular layer appears to be formed due to intensive polygonization. In the second stage, nucleation and coalescence of micro-debondings take place. Lastly, the penny-shape crack is formed.

Murakami et. al (2002) (Roiko and Murakami (2012), Li et al. (2016)), correlate the rough surface with the hydrogen trapped around inclusions, suggesting that, it results from hydrogen assisted fatigue crack growth. When the FGA is formed, crack propagation would occur only due to cyclic loading.

Another model, which was, proposed by Shiozawa et al. (2006) (Li et al. (2016)), is divided in two steps. First, spherical carbides within the matrix suffer dechoesion, initiating several microcracks which will then grow and coalesce, thus forming the FGA.

Studies regarding the formation mechanisms of FGA are not yet well established. However, several empirical equations were developed in order to quantify FGA size and to find out whether it is a part of crack nucleation and /or propagation in the fatigue process.

2.2. Empirical equations for FGA

The fractographic features of a specimen tested in VHCF are expected to be related to the cyclic loading parameters as well as the mechanical characteristic of the steel. Accordingly, numerous studies have been conducted regarding the relationship between FGA size, on the one hand, and applied stress amplitude, material's strength and hardness, on the other hand. Assuming FGA on the fracture surface to be approximately a circle, Yang et al. (2008) deduced the following expression

$$\varphi_{FGA} = 1240 \frac{1}{\sigma_y{}^{0,533}} \frac{1}{\sigma_a{}^2} \tag{1}$$

where φ_{FGA} is the estimated diameter of FGA, σ_y the yield stress and σ_a the applied stress amplitude. Both σ_y and σ_a are in MPA and φ_{FGA} is in meters. Although the above expression indicates that φ_{FGA} decreases as σ_y and σ_a increase, FGA size is much more strongly influences by variations in σ_a.

Another expression for the FGA size was obtained by Liu et al. (2011) in terms of σ_a and Vickers hardness HV as given below:

$$\sqrt{A_{FGA}} = \left[\frac{2(HV + 120)}{\sigma_a}\right]^6 \tag{2}$$

Here the FGA size is represented by $\sqrt{A_{FGA}}$, where A_{FGA} is the projected area, in μm^2, on the fracture surface normal to the applied stress. With HV in the kg/mm^2 and σ_a in MPa, $\sqrt{A_{FGA}}$ is obtained in μm. Although equations (1) and (2) have different forms, both of them indicate that the FGA size at a given stress amplitude is constant for a given steel and is also independent of the inclusion size at the crack origin (Li et al (2016)). An expression similar to that represented by equation (2) was proposed earlier by Murakami (2002). Instead of the factor 2 in the above expression, Murakami had in fact proposed a constant C equivalent to 1.43 for superficial cracks and 1.56 for internal crack initiation.

$$\sqrt{area_{FGA}} = \left[\frac{C(HV + 120)}{\sigma_a}\right]^6 \tag{3}$$

2.3. SIF range for internal cracks

Taking into account the fact that $\sqrt{area_{FGA}}$ is much smaller than the specimen cross section dimension, ΔK_{FGA} was estimated by Murakami (2002) using the following expression

$$\Delta K_{FGA} = 0.5\, \Delta\sigma \sqrt{\pi \sqrt{area_{FGA}}} \tag{4}$$

where $\Delta\sigma$ refers to applied stress range, which is equivalent to 2 σ_a for fully reversed loading.

ΔK_{FGA} has been considered by a number of investigators (Tanaka and Akiniwa (2002), Sakai et al. (2002), Lu et al. (2009)) to be equivalent to the threshold value for stable crack propagation, meaning that ΔK_{FGA} is considered to be a material parameter essentially independent of fatigue life. However, if one considers that the FGA represents a small crack, ΔK_{FGA} will be dependent on the FGA size, being approximately proportional to $area_{FGA}{}^{1/6}$ (Li et al (2010), Murakami and Matsunaga (2006)). According to Li et al. (2016), this discrepancy can be explained by considering that ΔK_{FGA} increases with the increase in FGA size up to a transition crack length above which crack propagation mechanism transfers from small crack to long crack, and henceforth ΔK_{FGA} will remain constant at ΔK_{thR}. Both transition crack length and ΔK_{thR} are dependent on the strength of the material. In fact, the higher the strength of the steel, the shorter the transition crack length and the lower ΔK_{thR} value (Chapetti et al. (2003), Chapetti (2010), Li et al. (2016)). For a short crack, though, the threshold value increases with increasing the material's hardness (Chapetti (2010)).

3. Material and Experimental Procedure

The material used in this study is a crankshaft steel, DIN34CrNiMo6. The machined specimens were obtained directly from crankshaft failed in service. The chemical composition and the mechanical properties of the steel are given respectively in Table 1 and 2. The steel has a density of 7.870 kg/cm^3 and its Vickers hardness amounts to 330 HV.

Table 1. Chemical compositions with main elements.

Steel: DIN34CrNiMo6				
Fe (%)	C(%)	Cr (%)	Mo(%)	Ni(%)
95.1	0.38	1.51	0.24	1.75

Table 2. Mechanical properties.

Steel: DIN34CrNiMo6		
σ_u (MPa)	σ_y(MPa)	E(GPa)
900	760	207

The fatigue specimen dimensions were based on the Bathias geometric principal (2005). This specimen has an hourglass shape and the dimensions depends on the density and modulus of elasticity. The resonance length obtained is 16.10 mm with a maximum diameter of 10 mm and a minimum diameter of 3 mm (Fig.2).

The specimens were submitted to ultrasonic fatigue test with loading conditions R= -1. The tests were carried out in the laboratories of Instituto Superior Técnico in Lisbon University. The fatigue analysis in the VHCF region was performed with the purpose of obtaining the behavior of the steel. After the tests, fracture surfaces were observed in SEM to identify the fish-eye and FGA regions. With the aid of DIP program, it was possible to define the texture of the initiation site and hence determine the size of fish-eye and FGA regions revealed by different coloration.

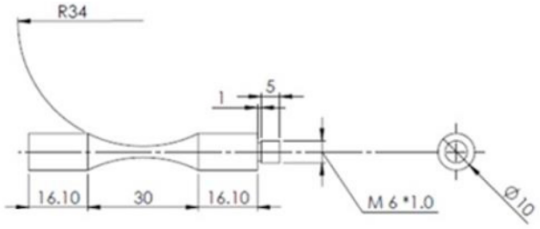

Fig. 2. Fatigue specimen hourglass shape with dimension in mm.

4. Results and discussion

The S-N curve obtained for the DIN34CrNiMo6 steel in the VHCF regime is presented in Figure 3.

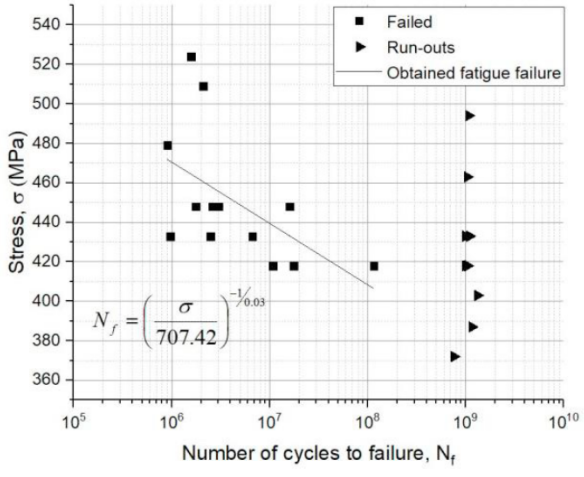

Fig. 3. S-N curve for the steel in question in the VHCF.

Seven specimens with fatigue life N_f pertaining to the range between 10^6 and 10^9 cycles were selected for fractographic examination in an effort to locate fatigue crack initiation sites. These specimens were labled from 1 to 7, and both their fatigue life N_f together with the corresponding applied stress amplitude σ_a are listed in Table 3. Examples of the relevant fractographic features encountered on the specimen fracture surfaces are shown in Fig. 4. and 5, where one can observe fatigue crack initiation at subsurface nonmetallic inclusions.

Table 3. Specimens selected for fractographic analysis.

Specimens n°	N_f	σ_a (MPa)
1	3,03E+06	448
2	6,69E+06	433
3	1,16E+08	418
4	1,58E+06	524
5	2,11E+06	509
6	1,60E+07	448
7	1,80E+07	418

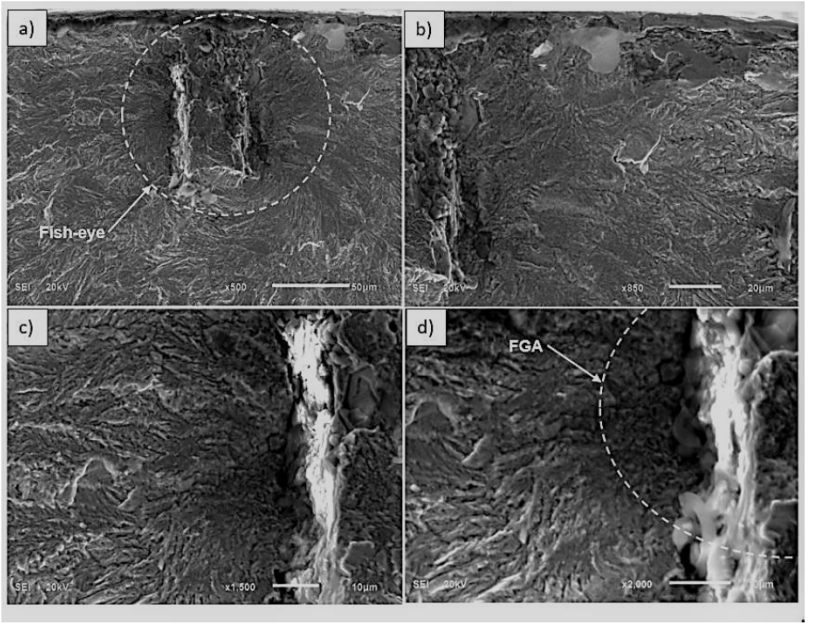

Fig. 4. SEM of the fracture surface of specimen n° 3: a) delineating fish-eye boundary; b) magnified left side of a; c) details of the right side in a; d) delineating FGA periphery.

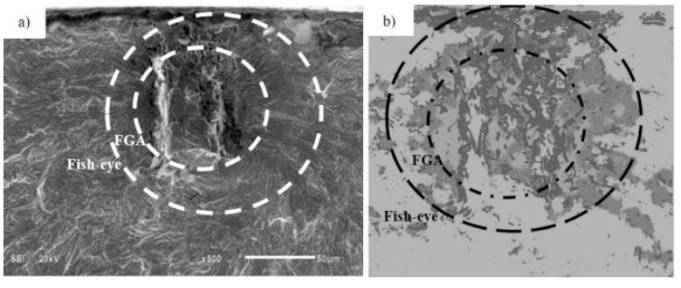

Fig. 5. Fish-eye and FGA regions as observed by: a) SEM; b) DIP.

The measured FGA size denominated d_{FGA} is presented in Fig.6, in comparison with φ_{FGA}, $\sqrt{A_{FGA}}$ and $\sqrt{area_{FGA}}$. Whereas φ_{FGA} was calculated using equation (1), $\sqrt{A_{FGA}}$ and $\sqrt{area_{FGA}}$ were estimated using equations (2) and (3) respectively.

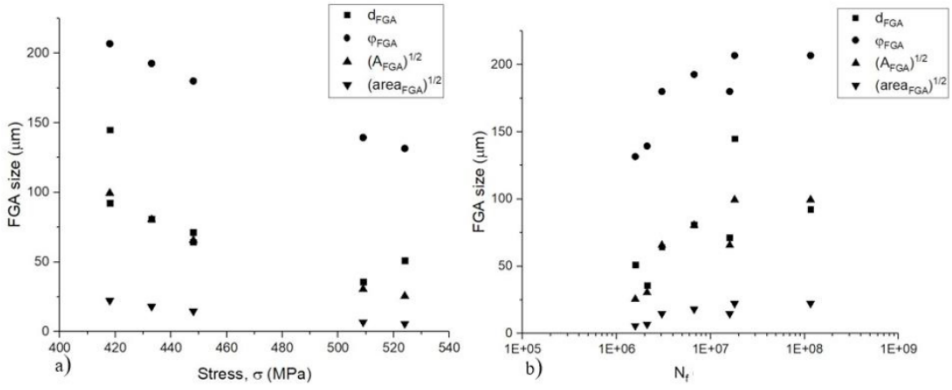

Fig. 6. Measured and calculated FGA size as functions of: a) stress amplitude; b) number of cycles to failure.

Based on this figure one may conclude that the measured FGA size agrees well with Liu´s formula (equation (2)), but only fairly with Murakami's equation (3). This is clearly shown in Fig. 7. where the percent difference between measured and calculated values of the FGA size is presented for the specimens in question.

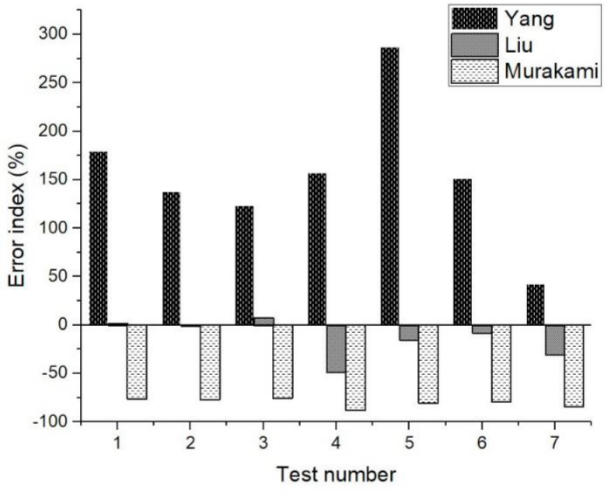

Fig. 7. Percent difference between measured and calculated FGA size.

4.1. SIF range at FGA periphery

The threshold for internal crack propagation used to be considered as equivalent to the threshold for long crack, ΔK_{thR}. Whereas ΔK_{thR} is a material constant for a given stress ratio R, the threshold for the propagation of internal short cracks depends on crack length. As proposed by Murakami and coworkers (2014), ΔK_{th} for this type of cracks can be estimated from the following expression

$$\Delta K_{th} = 2.77 \cdot 10^{-3}(HV + 120)\sqrt{area_{FGA}}^{1/3}; \quad \Delta K_{th} < \Delta K_{thR} \tag{5}$$

ΔK_{th} estimated using the above relationship is presented in Fig. 8, as a function of d_{FGA} except for the largest

FGA size, which showed a threshold value of approximately 9 MPa $m^{1/2}$. This threshold level is higher than ΔK_{thR} for DIN34CrNiMo6 steel, which is situated at only 7 MPa $m^{1/2}$. Accordingly, a transition FGA size from short to long crack is seen to exist at d_{FGA} of about 177.5 μm.

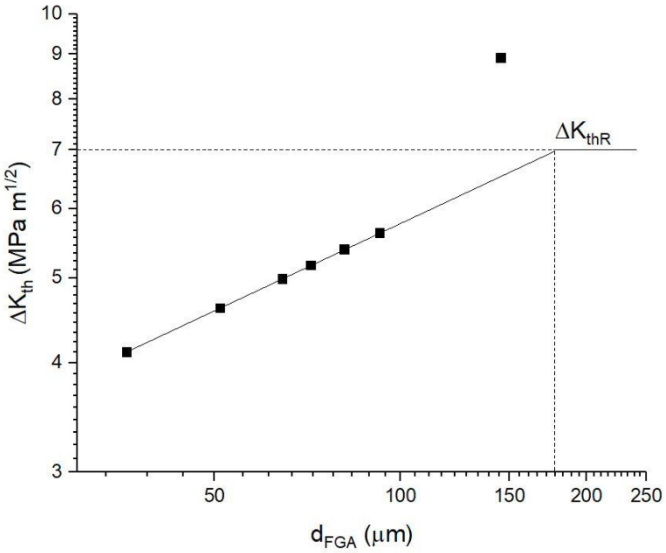

Fig. 8. ΔK_{th} as a function of FGA size.

Finally, the average values of ΔK at fish-eye and FGA boundaries are given in Fig.9.

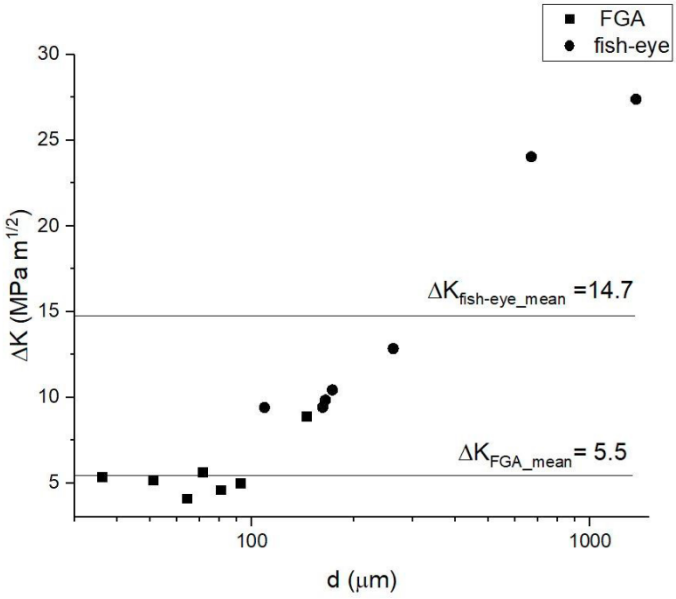

Fig. 9. Individual values of ΔK at fish-eye and FGA peripheries together with their corresponding average values.

5. Conclusions

From what is present above, the following conclusions can be drawn.

- Experimentally measured of FGA size agrees well with the relationship proposed by Liu et al. and fairly so with Murakami's expression.
- Taking into account the value of ΔK_{thR} for DIN34CrNiMo6 steel, a transitional FGA size from short to long crack is estimated at about 177.5 μm.

Acknowledgements

This work was developed within the scope of the Research and Technological Development of the Brazilian Electric Energy Sector Program regulated by ANEEL, with the support of the Eneva Companies - Pecém II Energy Generation S.A., Itaqui Energy Generation S.A. and Parnaíba I, II and III Energy Generation S.A.

References

Bathias, C. 2005. *Gigacycle Fatigue in Mechanical Pratice*. Academic Press.

Kazymyrovych, V. 2009. *Very High Cycle Fatigue of Engineering Materials - A Literature Review*. www.kau.se.

Kazymyrovych, V. 2008. "Very High Cycle Fatigue of High Performance Steels."

Kazymyrovych, V., J. Bergstrm, and C. Burman. 2010. "The Significance of Crack Initiation Stage in Very High Cycle Fatigue of Steels." *Steel Research International* 81(4): 308–14.

Li, Wei et al. 2015. "Subsurface Inclusion-Induced Crack Nucleation and Growth Behaviors of High Strength Steels under Very High Cycle Fatigue: Characterization and Microstructure-Based Modeling." *Materials Science and Engineering A* 641: 10–20.

Li, Yong De, Zhang Li-Li, Fei, Yu-Huan, Liu, Xiao-Yan, Li, Mei-Xia. 2016. "On the Formation Mechanisms of Fine Granular Area (FGA) on the Fracture Surface for High Strength Steels in the VHCF Regime." *International Journal of Fatigue* 82: 402–10.

Liu, Y B, S X Li, Y D Li, and Z G Yang. 2011. Factors Influencing the GBF Size of High Strength Steels in the Very High Cycle Fatigue Regime. "*Mater Sci Eng*" 358: 935–42.

Marines, I., X. Bin, and C. Bathias. 2003. "An Understanding of Very High Cycle Fatigue of Metals." *International Journal of Fatigue* 25(9–11): 1101–7.

Murakami, Y. 2002. Metal Fatigue : Effects of Small Defects and Nonmetallic Inclusions. Elsevier.

Murakami, Y, and Matsunaga, H. 2006. "The Effect of Hydrogen on Fatigue Properties of Steels Used for Fuel Cell System." *International Journal of Fatigue*" 28(11): 1509–20.

Ochi,Y, Matsamura,T , Masaki, K and Yoshida, S. 2002. "High-Cycle Rotating Bending Fatigue Property in Very Long-Life Regime of High-Strength Steels. *Fatigue and Fracture of Engineering Materials and Structures* (i): 1–5.

Pyttel, B., D. Schwerdt, and C. Berger. 2011. "Very High Cycle Fatigue - Is There a Fatigue Limit?" *International Journal of Fatigue* 33(1): 49–58.

Sakai, Tatsuo. 2009. "Review and Prospects for Current Studies on Very High Cycle Fatigue of Metallic Materials for Machine Structural Use." *Journal of Solid Mechanics and Materials Engineering* 3(3): 425–39.

Sakai, T, Sato Y, Oguma N. 2002. Characteristic S-N properties of high carbon-chromium bearing steel under axial loading in long life fatigue. Fatigue Fract Eng Mater Struct 25: 765–73

Shiozawa, K., Y. Morii, S. Nishino, and L. Lu. 2006. "Subsurface Crack Initiation and Propagation Mechanism in High-Strength Steel in a Very High Cycle Fatigue Regime." *International Journal of Fatigue* 28(11): 1521–32.

Tanaka K, Akiniwa Y, 2002. Fatigue crack propagation behavior derived from S-N data in very high cycle regime. *"Fatigue Fract Eng Mater Struc"* 25: 775-84.

Lu LT, Zhang JW, Shiozawa K, 2009. Influence of inclusion size on S-N curve characteristic of high strength steels in the gigacycle fatigue regime. "Fatigue Fract Eng Mater Struct " 32: 647-55.

Yang, Z G. 2008. Estimation of the Size of GBF Area on Fracture Surface for High Strength Steels in Very High Cycle Fatigue Regime. "International Journal of Fatigue" 30: 1016–23.

Li YD, Chen SM, Liu YB, Yang ZG, Li SX, Hui WJ, (2010). The characteristics of granular brigth facet in hydrogen pre-charged and un-charged high stregth steels in the very high cycle fatigue regime. *"J Mater Sci"* 45:831-41.

Chapetti MD, Tagawa T, Miyata T.(2003). Ultra-long cycle fatigue of high carbon steels part II: estimation of fatigue limit failure from internal inclusions.*"Mater Sci Eng"* 356: 236-44.

Murakami Y, Yamashita Y (2014). Prediction of Life Scatter of Fatigue Failure originated at nonmetallic Inclusions. *"Procedia Engineering"* 74: 6-11.

Chapetti MD (2010). Prediction of threshold for very high cycle fatigue ($N>10^7$) cycles. *"Procedia Engineering"*2: 257-64.